



Identifying spiral wave tips with reservoir computing

Yeyuge Chen^a, Xiaolongzi Wu^a, Yu Qian^b, Xiaohua Cui^{a,*}

^a School of Systems Science, Beijing Normal University, Beijing 100875, PR China

^b Nonlinear Research Institute, Baoji University of Arts and Sciences, Baoji 721007, PR China

ARTICLE INFO

Keywords:

Reservoir computing
Spiral waves
Tip identification
Topological structures

ABSTRACT

Identifying spiral wave tips of spatiotemporal dynamical systems from time series represents a significant challenge for understanding and controlling complex dynamics. Many previous methods for calculating tips relied on phase analysis, and they inevitably needed to set a phase origin and required multiple time slices for phase calculation. Reservoir computing, a simplified recurrent neural network paradigm, has spurred many investigations in several fields to capture and predict the features of complex, nonlinear dynamics. Based on the superior performance of reservoir computing, we investigated its application in analyzing spiral wave tips in reaction–diffusion systems. In this paper, we employ reservoir computing to identify spiral wave tips in some simple cases (spiral waves modeled by CGLE with one or two tips) and demonstrated that our model could accurately identify tips using only one time slice. Furthermore, we confirmed that the model maintained high accuracy in identifying tips of moving one-tip spiral waves in other systems (Bär, FHN). Moreover, we analyzed complex cases (evolving spiral waves and turbulence), with results indicating effective model performance. Ultimately, we demonstrated reservoir computing's robustness, noting its superior performance over conventional algorithms when handling data contaminated with noise from the sampling process. In summary, reservoir computing exhibits low computational complexity, requires minimal data and fewer constraints, and achieves high accuracy. This approach offers novel prospects for identifying topological structures in practical applications, such as monitoring and controlling spiral wave tips in cardiac illnesses.

1. Introduction

Spiral waves, whose mechanism is mainly caused by defects in space topological structure [1], are special and common spatial patterns that exist in many complex systems. Recently, research on spiral waves has gained significant attention, including the control of spiral waves [2,3], pinned spiral waves [4], tissue defects [1,5], spiral waves tip trajectories and their relevant stability or instability [6,7]. Among these topics, phase singularity (PS i.e. tips of spiral wave) identification has emerged as a crucial research area concerning spiral waves in the heart. Spiral waves can cause vascular arrhythmias, including ventricular tachycardia (VT) and ventricular fibrillation (VF), which are the primary causes of sudden cardiac death (SCD) each year [8,9]. Most arrhythmias originate from reentry, focal excitations, or a mixture of both [10,11]. The success rate of eliminating abnormal waves with stereotactic radio-frequency ablation [12,13] can be significantly improved by locating tip sites and identifying the types of abnormal waves. In practical experiments, temporal data from each spatial node are readily and conveniently acquired, and the utilization of spatiotemporal data for identifying spiral wave tips constitutes a prominent research focus. Several approaches have been investigated for identifying spiral wave

tips, including line integral method [14], convolution method [15], topological charge-density method [16], Jacobian determinant method (JM) [17], etc. However, a common issue with current methods for computing spiral wave tips is the lag time involved. This issue arises because data from a subsequent time interval are essential for calculating the tip position at a given moment. Specifically, data recorded up to time $t + \Delta t$ are required for calculating the tip location at time t . Tip calculations are highly sensitive to the length of the required data, which is not standardized. To overcome this limitation, we propose adopting machine learning to accurately identify spatial tips based on one time slice.

In the recent past, the utilization of artificial intelligence in spiral wave research has been progressively intensifying [18,19]. For instance, researchers have employed deep neural network (UNet) approaches to determine the positions of spiral wave tips. Nevertheless, such systems also have a lag issue, poor accuracy in certain situations, and extremely high computing costs [19]. Concerning technique selection, reservoir computing (RC) [20,21] has received widespread research interest attributed to its notable accuracy and efficiency advantages over other traditional methods in nonlinear science. For example,

* Corresponding author.

E-mail address: xhcui@bnu.edu.cn (X. Cui).

RC has been widely exploited to predict the evolution processes of nonlinear systems, as exemplified by the classic parallel RC method, successfully predicting up to 5–6 Lyapunov times in large-scale spatiotemporal chaotic systems [22]. Subsequently, a hybrid forecasting approach extended this prediction capability to 12 Lyapunov times [23]. Moreover, some studies have implemented special equations to “update” the input to obtain effective long-term predictions [24]. Recent research has focused on the dynamical properties of nonlinear systems, for instance, using the time series to determine a dynamical system’s Lyapunov exponents [25,26], crucial transitions [27,28], and sensing phase coherence [29]. Additionally, RC has been applied to identify chaotic signals [30,31], perform partial variable inference [32,33], synchronization [34,35], and dynamically observe excitable systems [36]. In light of this, we have opted to utilize reservoir computing for tip identification, and preliminary test results affirm its feasibility.

The paper is divided into 4 sections. Section 2 presents the proposed RC model, the related data processing approach and the error calculation algorithm. Section 3 investigates the availability of RC for identifying tips in simple spiral wave modes, explores the applicability and challenges encountered when examining evolving spiral waves and turbulence modes, and presents the influence of Gaussian white noise on the identification process. Section 4 draws the main conclusions.

2. Model

We modify the original RC structure [20,21] to identify the tip positions in nonlinear systems. The RC model is still composed of three parts: an I/R layer (sequence-to-reservoir), a reservoir ($\mathbf{R}(t)$), and a R/O layer (reservoir-to-point). The I/R layer is mainly used to map a lower-dimensional input vector into a higher-dimensional reservoir network. The input data is the distribution matrix of system variables at a certain time. The matrix \mathbf{W}_{in} used in the mapping process is randomly generated from a uniform distribution $[-1, 1]$ with a dimension of $D_r \times (D_{in} + 1)$. Once the input matrix \mathbf{W}_{in} is generated, it remains fixed throughout the subsequent locating phase. Eq. (1) updates the states of the nodes in the reservoir network:

$$\mathbf{r}(t + \Delta t) = (1 - \alpha)\mathbf{r}(t) + \alpha \tanh(\mathbf{A}\mathbf{r}(t) + \mathbf{W}_{in}(\mathbf{V}_S(t + \Delta t) + \xi)), \quad (1)$$

where \mathbf{W}_{in} is the weight matrix between the input layer and the reservoir layer. The reservoir layer’s weighted adjacency matrix \mathbf{A} is constructed from a sparse random ER matrix with a dimension of $D_r \times D_r$, where the average degree of the network is D and the fraction of nonzero matrix members is D/N . Wherein, nonzero element values are also randomly drawn from the interval $[-1, 1]$. The matrix \mathbf{A} is rescaled by its spectral radius ρ , and once selected, we keep it fixed. The reservoir network node states are represented by $\mathbf{r}(t)$, where $\mathbf{r} \in \mathbb{R}^{D_r}$, we set the initial conditions as 0 in the training phase. We substitute it into Eq. (1) to calculate $\mathbf{r}(t+1)$ for the next moment, then, the obtained $\mathbf{r}(t+1)$ is substituted into Eq. (1) to obtain the $\mathbf{r}(t+2)$, and we repeat the above processes iteratively. We discard the top 10 sets of data due to their significant fluctuations in calculating the output weight \mathbf{W}_{out} . In the locating phase, we input the last $\mathbf{r}(t)$ value in the training phase to run the reservoir for identifying spiral wave tips. The input vector is represented by the D_{in} -dimensional $\mathbf{V}_S(t)$, and the hyperbolic tangent function \tanh primarily modifies the input in a nonlinear way. During the calculation process, each node in the reservoir layer is updated at a rate of α , and ξ is the bias parameter. Unlike the classic RC structure, we modify the data structure from the reservoir to the output layer. For the R/O layer(reservoir-to-point), we select the output data as a zero-one matrix with the same dimension as the input data. Specifically, we choose the Jacobian determinant method (JM) to calculate the tip positions, set the tip points to 1, and set the remaining points to 0 to generate a position matrix, which is used as the target values $\mathbf{V}_L(t)$.

In the training phase, the primary goal is to obtain the weight matrix \mathbf{W}_{out} using the T_1 data (T_1 is the length of the training data), where the dimension of \mathbf{W}_{out} is $D_{out} \times (D_{out} + D_r + 1)$. Therefore, all

parameters that are based on matrices \mathbf{A} and \mathbf{W}_{in} are hyperparameters [37]. Some methods transfer nonlinearity from the reservoir to the output layer [38], in this paper, the output layer is selected to have a linear function to a matrix $\mathbf{R}(t)$. Here, we construct the matrix $\mathbf{R}(t) = [\mathbf{r}(t); \mathbf{V}_S(t); \xi]$ made up of the input $\mathbf{V}_S(t)$, the reservoir states $\mathbf{r}(t)$ and the bias parameter ξ . The output $\mathbf{V}_L(t)$ at time t is described by

$$\mathbf{V}_L(t) = \mathbf{W}_{out}\mathbf{R}(t). \quad (2)$$

The system is open during the training phase, and the output $\mathbf{V}_L(t)$ is obtained from the target values, which are calculated by JM. Here, we use ridge regression [39] to obtain the output weight \mathbf{W}_{out} by matching the output values to the target values in a least-square sense. To optimize the following hyperparameters: learning rate α , bias parameter ξ , training length T_1 , and number of reservoir nodes N , we employ the Grid Search technique. By defining the combination of candidate values for the hyperparameters, it thoroughly searches for every possible combination and assesses each combination’s performance on the validation set. Lastly, the optimal solution is determined by selecting the combination of hyperparameters that performs the best.

$$\mathbf{W}_{out} = \mathbf{V}_L(t)\mathbf{R}^T(\mathbf{R}\mathbf{R}^T + \eta\mathbf{I}), \quad (3)$$

where $\eta = 1 \times 10^{-8}$ is a deviation parameter used to prevent overfitting of \mathbf{W}_{out} . After training, the output weight matrix \mathbf{W}_{out} is obtained. In other words, the input weight matrix \mathbf{W}_{in} , the reservoir weight matrix \mathbf{A} and the output weight matrix \mathbf{W}_{out} are fixed, we can use the trained model to identify spiral wave tips.

In the locating phase, we select the time slice of the system variables at each moment for $t \in T_2 = 100$ (T_2 is the length of the testing data) as the input vector to obtain the corresponding spiral wave tip positions at time t . Typically, the RC model comprises two phases: training and locating, as depicted in Fig. 1. From Output to Receiver, we designate the positions of non-zero elements in the output vector as tips. However, the output data is a vector with values between 0 and 1, the lower value indicates that the probability of the corresponding point being a tip is fewer. Therefore, we remove the points whose values are extremely low from the non-zero elements in the output vector. Subsequently, tip positioning rules are modified: a non-zero element is selected as a tip if it is a local maximum and exceeds 0.5, while the remaining non-zero elements are set to 0. In evolving spiral waves and turbulence cases, the generation and disappearance of the number and positions of tips are rapid. The huge changes in these spiral wave systems cause the error to increase if the RC network is trained using the prior segment of the time series and then used to identify the tip positions in the following time. To solve this problem, we randomly shuffle all the time slices $\mathbf{V}_S(t)$ and their corresponding tip position vectors $\mathbf{V}_L(t)$, and reorganize them into a new sequence. Then, we train the RC network with the $T \in T_1$ part of the new sequence and identify the next 100 steps.

In this paper, we choose 100 slices of different-moment to test the accuracy of the trained model, the accuracy of each task is evaluated by two indicators: the number of accurate tip identifications(AC) and distance error(DE). We process the output data $\mathbf{V}_L(t)$ calculated by RC and this step is as follows. We select its local maximum value as the tips and divide them into $true_{RC}$ and $false_{RC}$ (the tips in a spatial range of ± 1 pixel of the tip calculated by JM are $true_{RC}$, and the other tips are $false_{RC}$). Similarly, we divide the tips calculated by JM into $true_{JM}$ and $false_{JM}$ (if a spiral wave tip yielded by JM has a counterpart in the tips calculated by RC (T_{RC}) within the spatial range of ± 1 , this tip counts as $true_{JM}$, and the other tips are $false_{JM}$). The specific calculation steps for the two indicators are shown in Algorithms 1 and 2. The accuracy of the model is subsequently evaluated using the average of the 100 sets.

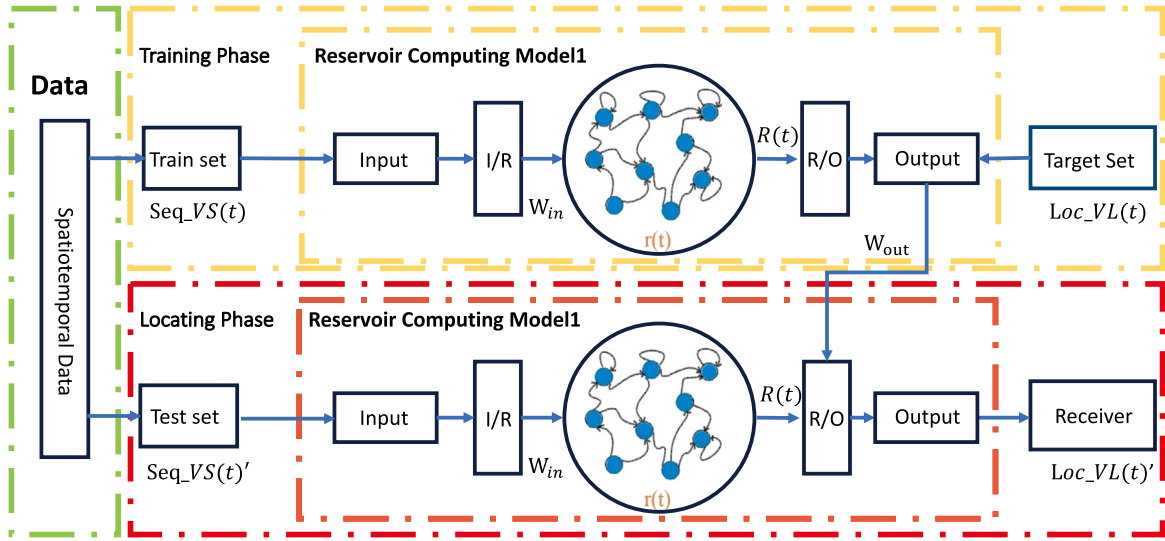


Fig. 1. The reservoir computing (RC) model's computation consists of training and locating phases. Comprising three components: an I/R layer, a reservoir, and a R/O layer. The I/R layer maps a lower-dimensional input vector to a higher-dimensional reservoir network, with the input weight W_{in} randomly assigned from a uniform distribution between $[-1, 1]$. The reservoir layer is constructed from a sparse random ER matrix, wherein, nonzero element values are also randomly drawn from the interval $[-1, 1]$. The R/O layer transforms a higher-dimensional reservoir network into a lower-dimensional output vector, necessitating the calculation of the output weight W_{out} during the training phase. (a) In the training phase, the input $V_S(t)$ and the output $V_L(t)$ are known, then the W_{out} is calculated. (b) In the locating phase, we put the variable of the spiral wave system for $t \in T_2$ as the input vector, and then we can get the tips of the corresponding spiral wave at time T_2 . Unlike the classic RC, the output is not used as the input for the next time and the data is diverse.

Algorithm 1 Accuracy of Phase Singularity Calculation

Input: T_{JM} : the tips calculated by JM;
 T_{RC} : the tips calculated by RC;
 $True_{RC}$: the T_{RC} tips in a spatial range of ± 1 pixel for T_{JM} ;
 $False_{RC}$: the rest of the T_{RC} tips beyond the $True_{RC}$;
 $True_{JM}$: the T_{JM} tip has a counterpart in the T_{RC} within the spatial range of ± 1 ;
 $False_{JM}$: the rest of the T_{JM} tips beyond the $True_{JM}$;
 n : the total number of lattice points in space;

Output: accuracy AC_{mean}

- 1: initial $AC_{mean} = 0$ and $T = 100$;
- 2: **for** $t < 100$ **do**
- 3: compute T_{RC} and T_{JM} ;
- 4: compute $True_{RC}$ and $True_{JM}$;
- 5: compute $False_{RC} = T_{RC} - True_{RC}$
- 6: compute $False_{JM} = T_{JM} - True_{JM}$
- 7: $AC = 1 - (False_{RC} + False_{JM})/n$
- 8: **end for**
- 9: **return** $AC_{mean} = \text{mean}(\sum_{t=1}^T AC)$

3. Results

We utilize RC to identify the positions of tips in several different spiral wave cases. These scenarios include different one-tip spiral wave cases generated by different reaction–diffusion (RD) systems (CGLE, Bär, FHN). Furthermore, an array of spiral wave types is investigated, arising from parameter variations within the CGLE system, encompassing one-tip, two-tip, evolving spiral waves, and turbulence. During the numerical simulation process, we set $dt = 0.01$ and the total time $T = 10^5$, and use the Euler method to generate the preliminary data needed for the RC model.

3.1. Availability in simple spiral wave modes

First, we apply RC to the simplest spiral wave situation, which only has one tip and hardly drifts in space. In this case, we choose

Algorithm 2 Algorithm for Calculating the Distance Error between the T_{JM} and the T_{RC}

Input: N_{JM} : the number of tips derived from JM;
 N_{RC} : the number of tips derived from RC;
 x^{JM} : the x-coordinate corresponding to T_{JM} ;
 x^{RC} : the x-coordinate corresponding to T_{RC} ;
 y^{JM} : the y-coordinate corresponding to T_{JM} ;
 y^{RC} : the y-coordinate corresponding to T_{RC} ;
 N : total number of test;

Output: distance error between the T_{JM} and the T_{RC} : DE_{mean}

- 1: initial $DE = 0$, $DE_{mean} = 0$ and $n = 0$;
- 2: **for** $N < 100$ **do**
- 3: **for** i in range(N_{RC}) **do**
- 4: **for** j in range(N_{JM}) **do**
- 5: $\Delta x = x_i^{RC} - x_j^{JM}$
- 6: $\Delta y = y_i^{RC} - y_j^{JM}$
- 7: $D = \sqrt{\Delta x^2 + \Delta y^2}$
- 8: **end for**
- 9: $DE = DE + \text{Min}(D)$
- 10: **end for**
- 11: $DE = DE/N_{RC}$
- 12: **end for**
- 13: **return** $DE_{mean} = DE/100$

the complex Ginzburg–Landau equation (CGLE) to simulate the spiral wave, and the parameters are listed in the Supplementary Materials [40]. Through training, we successfully realize the positioning of the one-tip case, and its calculation accuracy (AC_{mean} in Algorithms 1) is maintained at approximately 100% within the error range of 1 pixel. (Without special instructions, the AC_{mean} remains the same definition.) We use the data consisting of $V_S = (\text{real}(W))^{T_1}$ and $V_L = (Tips)^{T_1}$ to train the reservoir ($T_1 = 1200$). The hyperparameters of the reservoir network are listed in Table 1. After training, we put the V'_S and obtain the corresponding tip positions V'_L ($T_2 = 100$). In Fig. 2(a), we display the results of RC and JM, and it is clear that the precision of the calculation is quite successful. Moreover, the results are effectively maintained in other one-tip conditions of CGLE. Comparing the results

Table 1

The hyperparameters of the reservoir network in different cases.

System	Case	Reservoir nodes (N)	Bias (ξ)	Spectral radius (ρ)	T_2	T_1
CGLE	One-tip	5000	0.1	70.4	100	1200
	Two-tip					2500
FHN	Spiral chimeras					4000
Bär	Reentry					3000
CGLE	Evolving spiral waves	7000	0.1	83.5	100	8000
	Turbulence					2000

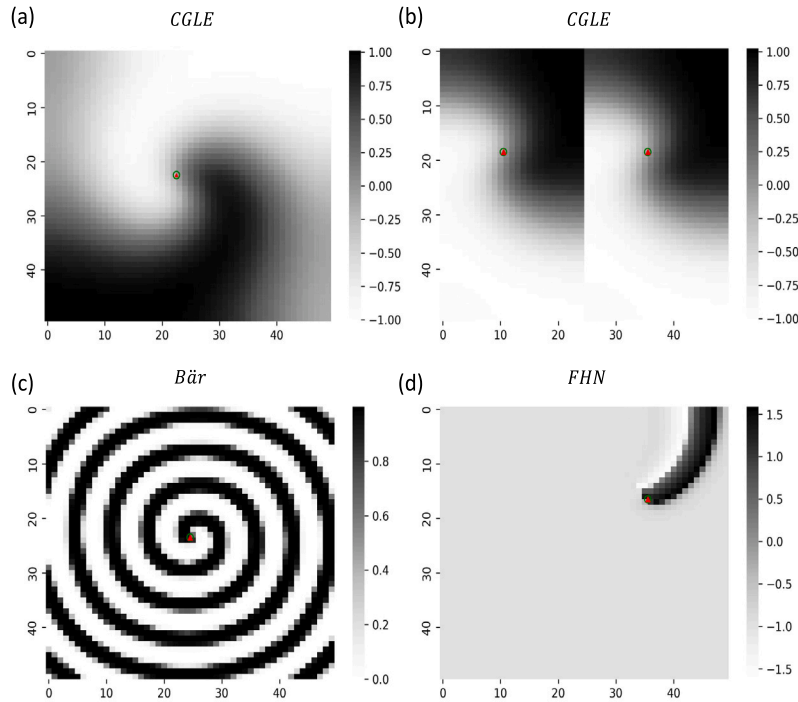


Fig. 2. A comparison of spiral wave tips identified by Jacobian determinant method (JM) and RC for CGLE, Bär and FHN are displayed ((a–d), respectively). Here, the corresponding tips calculated by JM are shown by green hollow circles, and tips calculated by RC are shown by red solid triangles. Subplot (a) shows the result of the one-tip mode, where the tip is chosen by the non-zero element which is the local maximum value. The results of two-tip case within the CGLE system are shown in subplot (b). Subplot (c) displays the results of the tip rotating around the center under the Bär system. The computed results of spiral chimeras under the FHN are shown in subplot (d). Overall, the identification of spiral wave tips coincides well with the target values. (Without special instructions, the green hollow circles and red solid triangles remain the same definition.) (For interpretation of the references to color in this figure legend, the reader is referred to the web version of this article.)

derived from RC and JM, we can easily find that there is no difference between them, and the distance error (DE_{mean} in Algorithms 2) for the 100 different runs is nearly 0.

After successfully utilizing the one-tip case, we use RC to calculate the tips in a more complicated two-tip mode. We discover that the trained RC model is also capable of identifying the tips in two-tip case, and the specific steps are listed below. By setting appropriate parameters (specifically listed in the Supplementary Materials), we can simulate the two-tip case and generate the experimental data. Similarly, in this case, the specific settings of hyperparameters are also shown in Table 1. Fig. 2(b) presents the results obtained in two-tip case, we can see that the tips derived from RC and JM perfectly coincide. By calculating 100 time slices, we obtain the relevant AC_{mean} value of 99.99%, which is nearly 100%. The DE_{mean} value is 0.1, which is smaller than half a pixel and far less than the system size. This indicates that the RC model is still suitable for the two spiral wave tips mode.

In Fig. 2(c), we randomly show an example to compare RC and JM in the reentry case by simulating the Bär [41] model, whose tip rotates around a circle (The relevant parameters are listed in the Supplementary Materials). It is apparent that the tip position can be precisely identified using the trained RC model. Additionally, we examine the spiral chimeras produced by an FHN system [42], in which the tip does not revolve around a regular circle. Here, we randomly select

the result for $t = 11$ to display in Fig. 2(d). Similarly, the red solid triangle calculated by RC perfectly falls within the green hollow circle calculated by JM. This reflects the good identification ability for spiral wave tips of RC. Moreover, these moving spiral waves are similar to anatomical reentry in cardiac illnesses [43], which rotate around obstacles in the heart. They typically occur in the tricuspid annulus of the atrium and may lead to reentrant tachycardia. Our findings show that RC can also be perfectly competent in these circumstances, and it has some practical implications for the identification and ablation of spiral wave tips in cardiac issues.

Finally, we compare the outcomes of three different systems for one tip, as shown in Fig. 3. Here, we perform 10 experiments again (each for 100 slices), each time using a different time slice and the same trained model. The RC model successfully settles these three systems, and it can accurately identify the tip position with the average accuracy AC_{mean} exceeding 99.99% and the average distance error DE_{mean} staying within 0.05 pixel. Even the poorest FHN system has a minimum accuracy AC_{mean} of 99.9992% and a maximum distance error DE_{mean} of 0.0932. This may be due to the complex tip trajectory which is an evolving spiral wave. In addition, these results indicate that the model has good robustness for different systems, and imply that it may be feasible for other models.

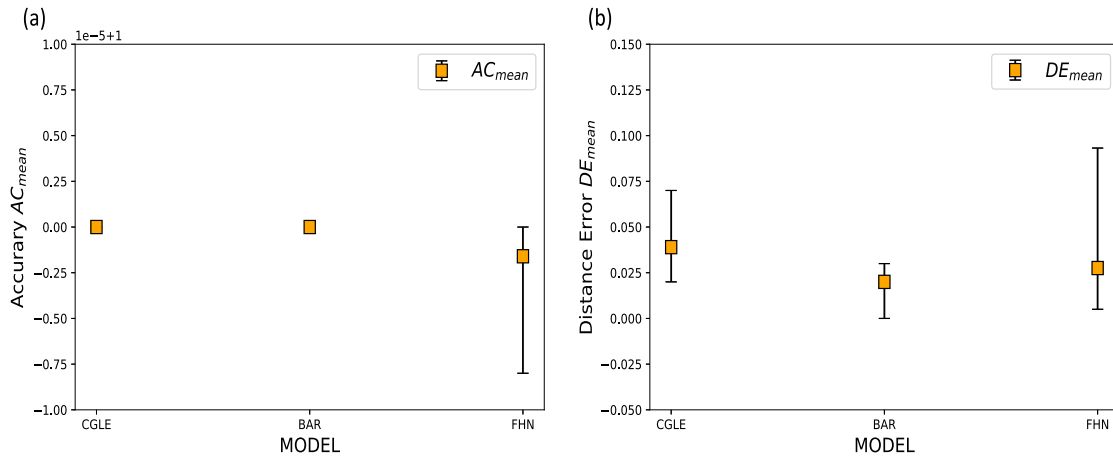


Fig. 3. The results of accuracy (AC) and distance error (DE) are calculated by 10 experiments again in three different one-tip systems, each time using 100 different time slices and the same trained model ((a), (b), respectively). Even the poorest FHN system has a minimum accuracy AC_{mean} of 99.9992% and a maximum distance error DE_{mean} of 0.0932. Overall, the average accuracy AC is greater than 99.99%, and the average distance error DE_{mean} stays within 0.05 for all systems. It is demonstrated that the RC model makes these three systems feasible.

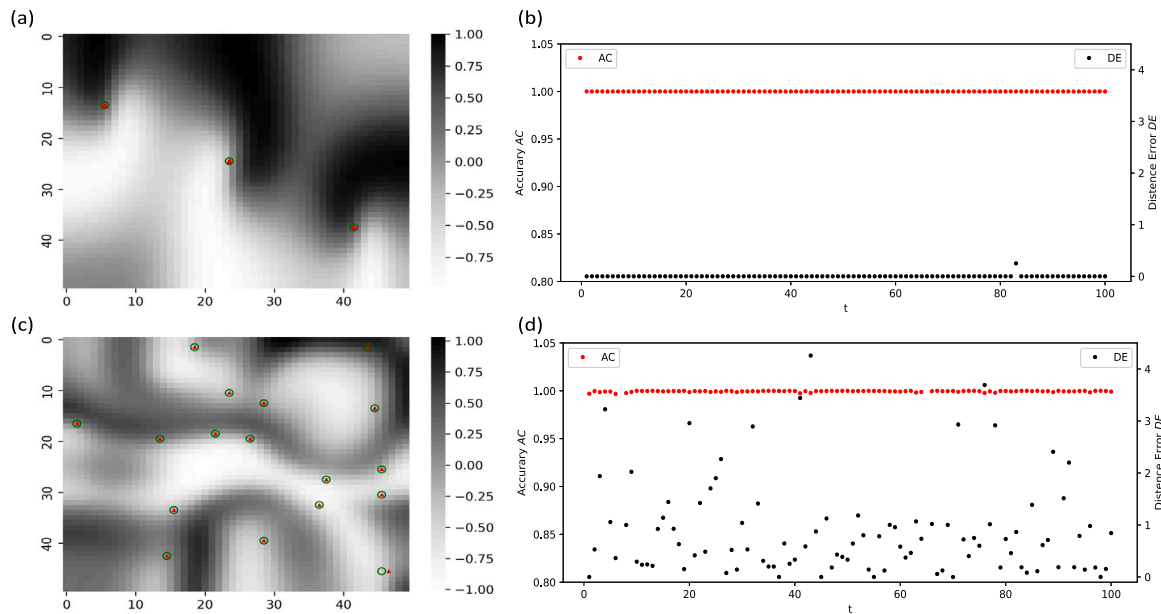


Fig. 4. Comparison of spiral wave tips identified by the conventional method (JM) and by the RC for evolving spiral waves and turbulence are shown in subplots (a), (c), respectively. (a), (c) illustrate that the tip positions (green hollow circle) calculated by JM method and the results obtained by RC model (red solid triangles) are highly consistent. (b) and (d) show the distribution of accuracy AC and distance error DE calculated from 100-time slices under evolving spiral waves and turbulence. Wherein, the red dot indicates accuracy AC , and the black dot indicates distance error DE . In (b), the red dots (AC) are maintained at about 1, indicating that the accuracy of the calculation results is maintained at 100% within the error range of 1 pixel. Besides, it can be seen that the black points (DE) are nearly 0, except for a time slice with $DE = 0.2$ pixel when $t = 83$. In (d), the majority of the red dots still appear to be nearly 1. Meanwhile, the distance error of RC mostly remains below 1 despite some fluctuations, and the average value $DE_{mean} = 0.89$, is much smaller than the system size ($N = 50$). (For interpretation of the references to color in this figure legend, the reader is referred to the web version of this article.)

3.2. Applicability and challenges in evolving spiral waves and turbulence modes

Moreover, complex systems have some unstable intermediate processes, such as continuously generating and breaking spiral waves. In this case, we test RC in similar situations by using the CGLE system, the specific parameters are listed in the Supplementary Materials. Unlike the two-tip case, we use the intermediate process of two tips evolving into one tip to simulate this situation, which has multiple dynamic tips and is referred to as evolving spiral waves. In Fig. 4(a), it can be seen that three tip positions (green hollow circle) are calculated by JM, while the results obtained by RC model also include three tips (red solid triangles), and their positions are highly consistent with the JM results. This proves that tips can still be precisely identified using the RC model

even in the evolving spiral waves case. Additionally, we calculate the AC and DE of this case, and the specific results are shown in Fig. 4(b). We can see that the red dots (AC) are maintained at approximately 1, indicating that the accuracy of the calculation results is maintained at 100% within an error range of 1 pixel. Besides, the black points (DE) are nearly 0, except for a time slice with $DE = 0.2$ pixel when $t = 83$. This demonstrates that the accuracy of RC calculation results is very high and has significant implications for applying RC to more complex situations involving more tips and faster position changes.

We next demonstrate that the RC model can be expanded to a turbulent system. The CGLE system transitions from simple spiral waves to turbulence when the coupling strength reaches a certain value [44]. The data corresponding to turbulence are obtained by setting the appropriate parameters of CGLE system (listed in the Supplementary

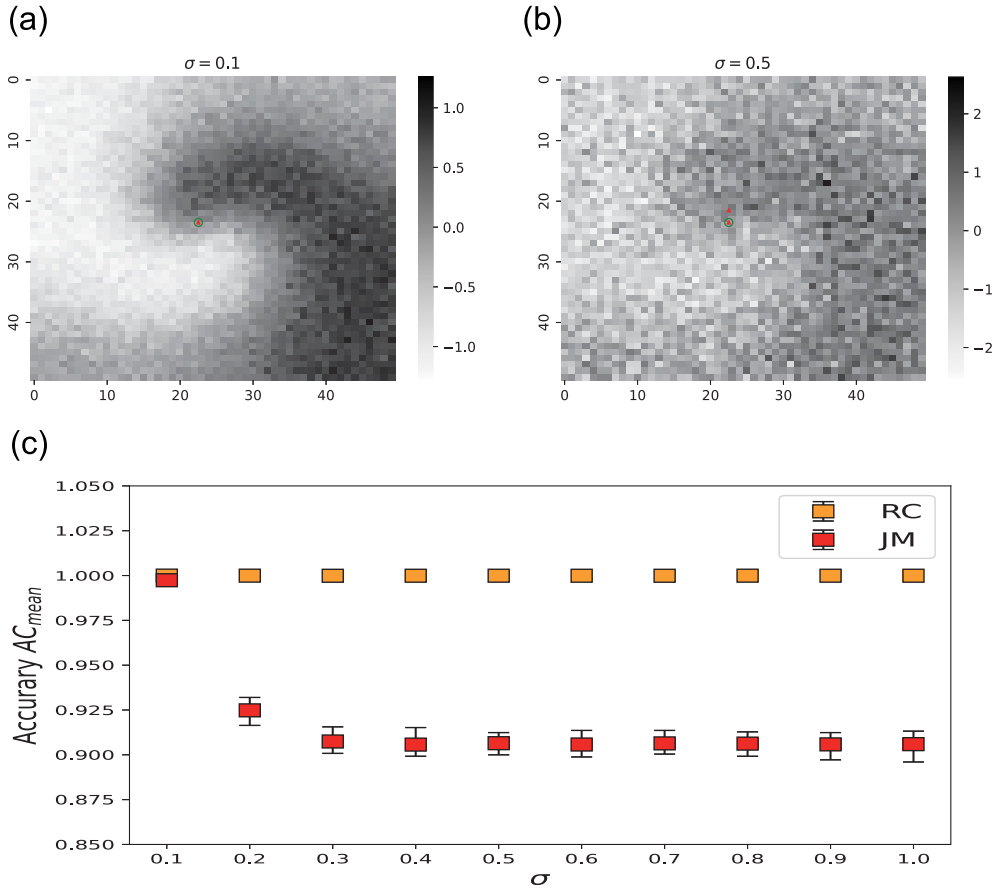


Fig. 5. The influence of additive Gaussian white noise on identifying tips. In subplots(a, b), an exemplary snapshot of variable real(W) (CGLE model) is shown for different noise intensities $\sigma = 0.1, 0.5$, respectively. When $\sigma = 0.1$, the results of RC are perfectly consistent with JM. As the noise intensity rises, there are some fluctuations in the calculation results, two tips can be formed close to the target value when $\sigma = 0.5$. In subplot (c), the accuracy AC is depicted which is calculated from JM (red bar) and RC (yellow bar), depending on σ . The error bar represents the maximum and minimum values of every 100 time slices. The results illustrate that the accuracy of the RC model (AC_{mean}) declines within a narrow range as the noise intensity σ rises. In contrast, for the traditional JM, AC_{mean} is roughly at the same level as that of the RC model initially and then decreases sharply after exceeding 0.2 before remaining constant. (For interpretation of the references to color in this figure legend, the reader is referred to the web version of this article.)

Materials). Similarly, we use the same processing approach mentioned in Section 2 to process the output data. Here, we randomly choose an example for conducting the comparison between RC and JM, and the results are displayed in Fig. 4(c). The change rate of the tips becomes more complex than the previous cases, but surprisingly, the majority of the red dots (AC) in Fig. 4(d) still appear to be approximately 1. This means the calculation accuracy AC of the RC model in the turbulence case is nearly consistent with the evolving spiral waves. We can see that the distance error DE (black dots) of RC mostly remains below 1 despite some fluctuations, and the average value $DE_{mean} = 0.89$. This result is much smaller than the system size ($N = 50$), although it looks larger than the DE in Fig. 4(b). In addition, we once again verify the feasibility of the RC model in most conditions. This model identifies the tip positions in all 100 time slices, except time-sliced data ($t = 8, 63$). We use the 98 time slices which the tips are identified to calculate DE_{mean} .

3.3. The influence of Gaussian white noise in the identification

In experiments, measurement inaccuracies unavoidably exist when data are recorded. To test the robustness of the proposed model, we consider adding Gaussian white noise to the input variable $V_S(t)$ to replicate noise during data recording. In other words, we add white noise ξ to each time slice and use $V_S(t) + \xi$ to replace the original $V_S(t)$ for calculating tip positions. (the white noise intensity is represented by σ .)

Fig. 5(a), (b) display the results of adding different noise intensities to the one-tip case at $t = 20$. They are the same time slice with noise intensities $\sigma = 0.1$ and $\sigma = 0.5$, respectively. We can see that when $\sigma = 0.1$, the model can accurately calculate the tip position in Fig. 5(a). However, as the noise intensity rises, some fluctuations are observed in the calculation results, and two tips can be formed close to the target value, as shown in Fig. 5(b). To demonstrate the accuracy of RC, we calculate the trends exhibited by JM and RC as the noise level varies. In Fig. 5(c), the results illustrate that the accuracy of the RC model (AC_{mean}) declines within a narrow range as the noise intensity σ rises. In contrast, for the traditional JM, AC_{mean} is roughly at the same level as that of the RC model initially and then decreases sharply after exceeding 0.2 before remaining constant. This demonstrates that the RC model outperforms traditional methods in terms of robustness for spiral wave tip identification.

Similarly, we conduct calculations for the evolving spiral waves case. We randomly select the time slice of $t = 3$ for display in Fig. 6(a-d), and the results correspond to noise intensities of $\sigma = 0, 0.1, 0.5$, and 1.0. In Fig. 6(a), the RC results are perfectly consistent with JM. When the noise intensity $\sigma = 0.1$, the AC remains at 100%, and the tip position results of RC are robust, as shown in Fig. 6(b). As the noise intensity further increases, the AC slightly decreases, and the tips identified by RC are near the target values, as shown in Fig. 6(c). When the noise intensity reaches 1.0, RC can still identify most of the tips within a certain range of error, although the ability of RC to identify tips is significantly reduced, as shown in Fig. 6(d). We calculate the trends for both JM and RC as the noise intensity varies in Fig. 6(e). It

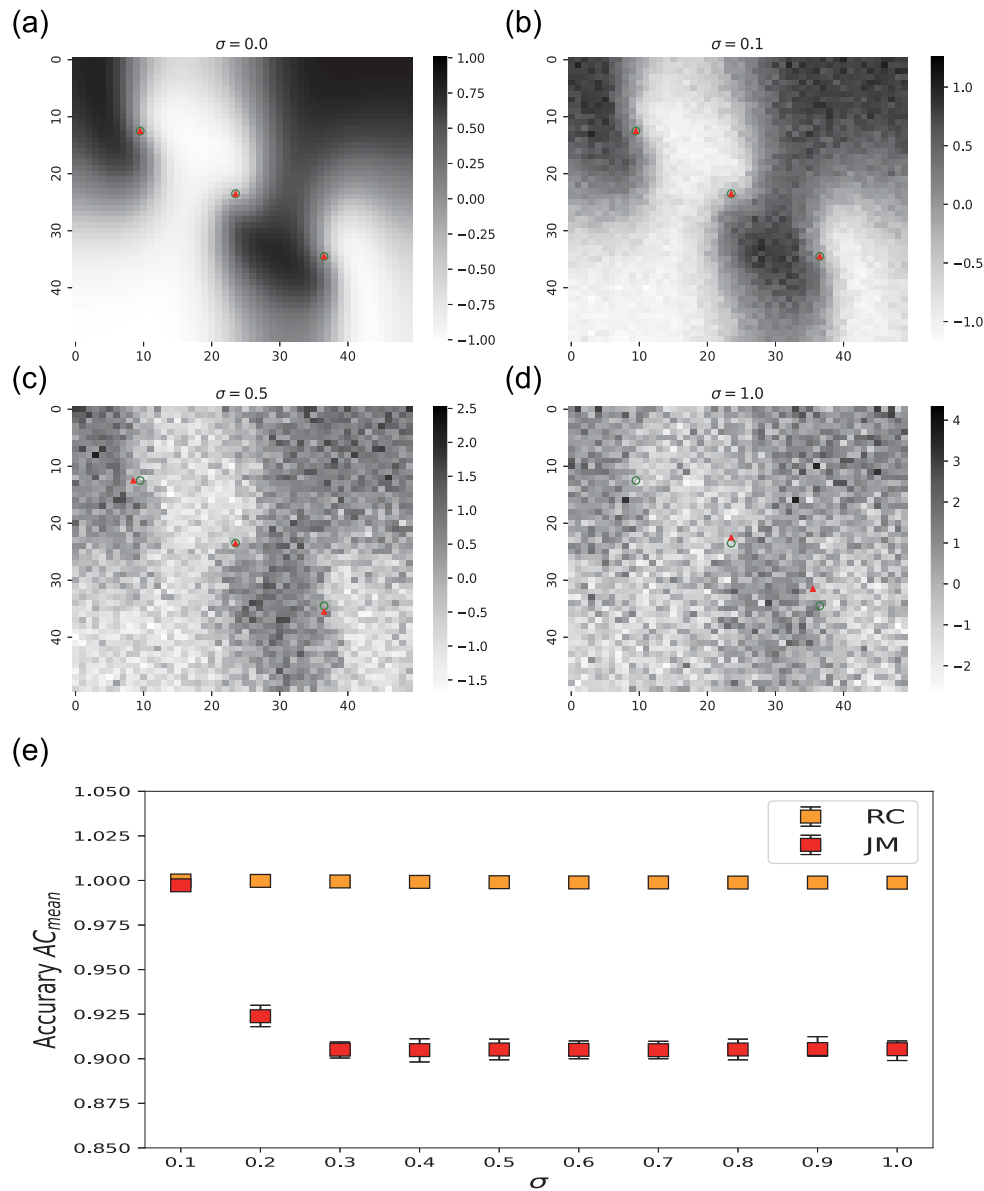


Fig. 6. In subplots (a–d), an exemplary snapshot is shown for different noise intensities $\sigma = 0.1, 0.5, 1.0$, respectively. As the noise intensity increases, the accuracy of tip identification gradually decreases. The accuracy of RC decreases as the identifying tips from three highly accurate points to two points with deviation. Subplot (e) shows the variation diagram of RC and JM affected by white noise intensity (σ) under the evolving spiral waves case. It is obvious that as the noise intensity increases, the AC_{mean} of the RC model fluctuates, but it still remains approximately 1. Meanwhile, AC_{mean} for JM significantly decreased with the increase until stabilizing at 0.9.

is obvious that as the noise intensity increases, the accuracy AC_{mean} is slightly decreased compared to that attained in the one-tip case, but it still approaches 1. However, the AC_{mean} of JM significantly decreases as σ increases until stabilizing at 0.9 (according to the system size of 50×50 , each time slice corresponds to 2500 points, and an accuracy of 0.9 indicates that approximately 250 points are incorrect, which is very large compared to the number of tips). In comparison, RC still maintains better robustness than JM for the other time slices. From the results obtained in the above two situations, it is evident that the RC model is more suitable for identifying the tip positions under noise.

4. Conclusions

In this paper, we use a modified RC model to identify tips from different data generated by various RD systems. Firstly, the RC model is used to identify tips in simple cases (spiral waves modeled by CGLE with one or two tips), as shown in Fig. 2(a), (b). The results show that the accuracy AC is nearly 100% and the distance error DE is below

0.1. Secondly, the RC model also exhibits extreme tip identification accuracy for the moving one-tip spiral wave cases involving other different systems (Bär, FHN), as shown in Fig. 2(c), (d) and Fig. 3. Thirdly, RC model is also used to identify the tips of more complex cases, such as evolving spiral waves and turbulence. The results reveal that the RC model is still valid in most conditions, as shown in Fig. 4. Finally, we use RC model to identify tips that have perturbation when recorded. The results show that RC model is more robust than JM in terms of identifying tips under noise, as illustrated in Figs. 5,6.

Overall, the modified RC model has huge advantages regarding tip identification. Firstly, RC model reduces the computational difficulty of identifying, as it only needs one time slice instead of multiple time slices before. Secondly, for multivariate systems, RC model only needs one variable's data to identify tips while the previous system needs 2 variables at least. Thirdly, it is robust as it does not need an initial phase point while other methods do. Finally, RC exhibits a stronger robustness when the data are polluted by noise than former JM does. Further investigation into the proposed RC approach has the potential

to expand our understanding significantly in identifying topological structures. Additionally, this facilitates the provision of recommendations for practical applications. For instance, in cardiac care, the RC model could be utilized to monitor and pinpoint tip positions in real time, potentially predicting the onset of spiral wave disruptions.

CRedit authorship contribution statement

Yeyuge Chen: Conceptualization, Formal analysis, Methodology, Validation, Writing – original draft, Writing – review & editing. **Xiaolongzi Wu:** Conceptualization, Writing – review & editing. **Yu Qian:** Conceptualization, Funding acquisition, Methodology, Writing – review & editing. **Xiaohua Cui:** Conceptualization, Formal analysis, Methodology, Supervision, Writing – original draft, Writing – review & editing.

Declaration of competing interest

The authors declare that they have no known competing financial interests or personal relationships that could have appeared to influence the work reported in this paper.

Data availability

Data will be made available on request.

Acknowledgments

The authors thank Chunli Huang for providing model data for CGLE system. This work is supported by the Natural Science Basic Research Plan in Shaanxi Province of China (Grant No. 2022JZ-03), and the Shaanxi Fundamental Science Research Project for Mathematics and Physics (Grant No. 22JSY021). We also want to express our gratitude for the helpful discussions among the students in our group.

Appendix A. Supplementary data

Supplementary material related to this article can be found online at <https://doi.org/10.1016/j.chaos.2024.114579>.

References

- [1] Hildebrand M, Bär M, Eiswirth M. Statistics of topological defects and spatiotemporal chaos in a reaction-diffusion system. *Phys Rev Lett* 1995;75(8):1503. <https://doi.org/10.1103/PhysRevLett.75.1503>.
- [2] Zhang H, Hu B, Hu G. Suppression of spiral waves and spatiotemporal chaos by generating target waves in excitable media. *Phys Rev E* 2003;68(2):026134. <https://doi.org/10.1103/PhysRevE.68.026134>.
- [3] Cao Z, Li P, Zhang H, Xie F, Hu G. Turbulence control with local pacing and its implication in cardiac defibrillation. *Chaos* 2007;17(1). <https://doi.org/10.1063/1.2713688>.
- [4] Chen J-X, Peng L, Ma J, Ying H-P. Liberation of a pinned spiral wave by a rotating electric pulse. *Europhys Lett* 2014;107(3):38001. <https://doi.org/10.1209/0295-5075/107/38001>.
- [5] Ma J, Xu Y, Tang J, Wang C. Defects formation and wave emitting from defects in excitable media. *Commun Nonlinear Sci Numer Simul* 2016;34:55–65. <https://doi.org/10.1016/j.cnsns.2015.10.013>.
- [6] Fenton FH, Cherry EM, Hastings HM, Evans SJ. Multiple mechanisms of spiral wave breakup in a model of cardiac electrical activity. *Chaos* 2002;12(3):852–92. <https://doi.org/10.1063/1.1504242>.
- [7] Ma J, Jia Y, Wang C-N, Li S-R. The instability of the spiral wave induced by the deformation of elastic excitable media. *J Phys A* 2008;41(38):385105. <https://doi.org/10.1088/1751-8113/41/38/385105>.
- [8] Virmani R, Burke AP, Farb A. Sudden cardiac death. *Cardiovasc Pathol* 2001;10(5):211–8. [https://doi.org/10.1016/S1054-8807\(01\)00091-6](https://doi.org/10.1016/S1054-8807(01)00091-6).
- [9] Myerburg R, Kessler K, Interian J, Fernandez P, Kimura S, Kozlovskis P, Furukawa T, Bassett A, Castellanos A. Cardiac electrophysiology: From cell to bedside. Vol. 1, Philadelphia: Saunders; 2004, p. 666–78. <https://doi.org/10.1161/01.CIR.0000146800.76451.65>, chapter Clinical and experimental pathophysiology of sudden cardiac death.
- [10] Qu Z, Weiss J. Mechanisms of cardiac arrhythmias. *Annu Rev Physiol* 2015;77. <https://doi.org/10.1146/annurev-physiol-021014-071622>.
- [11] Aras K, Kay M, Efimov I. Ventricular fibrillation: Rotors or foci? Both!. *Circ: Arrhythm Electrophysiol* 2017;10:e006011. <https://doi.org/10.1161/CIRCEP.117.006011>.
- [12] Haïssaguerre M, Jais P, Shah DC, Takahashi A, Clémenty J. Spontaneous initiation of atrial fibrillation by ectopic beats originating in the pulmonary veins. *N Engl J Med* 1998;339(10):659–66. <https://doi.org/10.1056/NEJM199809033391003>.
- [13] Calkins H, Hindricks G, Cappato R. 2017 HRS/EHRA/ECAS/APHS/SOLAECE expert consensus statement on catheter and surgical ablation of atrial fibrillation. *Heart Rhythm* 2017;14(10):e275–444. <https://doi.org/10.1093/europace/eux274>.
- [14] Goryachev A, Kapral R. Spiral waves in chaotic systems. *Phys Rev Lett* 1996;76(10):1619. <https://doi.org/10.1103/PhysRevLett.76.1619>.
- [15] Bray M-A, Lin S-F, Aliev RR, Roth BJ, Wikswo Jr JP. Experimental and theoretical analysis of phase singularity dynamics in cardiac tissue. *J Cardiovasc Electrophysiol* 2001;12(6):716–22. <https://doi.org/10.1046/j.1540-8167.2001.00716.x>.
- [16] He Y-J, Li Q-H, Zhou K, Jiang R, Jiang C, Pan J-T, Zheng D, Zheng B, Zhang H. Topological charge-density method of identifying phase singularities in cardiac fibrillation. *Phys Rev E* 2021;104(1):014213. <https://doi.org/10.1103/PhysRevE.104.014213>.
- [17] Li T-C, Pan D-B, Zhou K, Jiang R, Jiang C, Zheng B, Zhang H. Jacobian-determinant method of identifying phase singularity during reentry. *Phys Rev E* 2018;98(6):062405. <https://doi.org/10.1103/PhysRevE.98.062405>.
- [18] Ma J, Xu Y, Ren G, Wang C. Prediction for the breakup of spiral wave in a regular neuronal network. *Nonlinear Dynam* 2016;84:497–509. <https://doi.org/10.1007/s11071-015-2502-6>.
- [19] Lilienkamp H, Lilienkamp T. Detecting spiral wave tips using deep learning. *Sci Rep* 2021;11(1):19767. <https://doi.org/10.1038/s41598-021-99069-3>.
- [20] Jaeger H, Haas H. Harnessing nonlinearity: Predicting chaotic systems and saving energy in wireless communication. *science* 2004;304(5667):78–80. <https://doi.org/10.1126/science.1091277>.
- [21] Maass W, Natschläger T, Markram H. Real-time computing without stable states: A new framework for neural computation based on perturbations. *Neural Comput* 2002;14(11):2531–60. <https://doi.org/10.1162/08997660276047955>.
- [22] Pathak J, Hunt B, Girvan M, Lu Z, Ott E. Model-free prediction of large spatiotemporally chaotic systems from data: A reservoir computing approach. *Phys Rev Lett* 2018;120(2):024102. <https://doi.org/10.1103/PhysRevLett.120.024102>.
- [23] Pathak J, Wikner A, Fussell R, Chandra S, Hunt BR, Girvan M, Ott E. Hybrid forecasting of chaotic processes: Using machine learning in conjunction with a knowledge-based model. *Chaos* 2018;28(4):041101. <https://doi.org/10.1063/1.5028373>.
- [24] Fan H, Jiang J, Zhang C, Wang X, Lai Y-C. Long-term prediction of chaotic systems with machine learning. *Phys Rev Res* 2020;2(1):012080. <https://doi.org/10.1103/PhysRevResearch.2.012080>.
- [25] Sano M, Sawada Y. Measurement of the Lyapunov spectrum from a chaotic time series. *Phys Rev Lett* 1985;55(10):1082. <https://doi.org/10.1103/PhysRevLett.55.1082>.
- [26] Pathak J, Lu Z, Hunt BR, Girvan M, Ott E. Using machine learning to replicate chaotic attractors and calculate Lyapunov exponents from data. *Chaos* 2017;27(12):121102. <https://doi.org/10.1063/1.5010300>.
- [27] Kong L-W, Fan H-W, Grebogi C, Lai Y-C. Machine learning prediction of critical transition and system collapse. *Phys Rev Res* 2021;3(1):013090. <https://doi.org/10.1103/PhysRevResearch.3.013090>.
- [28] Saha S, Mishra A, Ghosh S, Dana SK, Hens C. Predicting bursting in a complete graph of mixed population through reservoir computing. *Phys Rev Res* 2020;2(3):033338. <https://doi.org/10.1103/PhysRevResearch.2.033338>.
- [29] Zhang C, Jiang J, Qu S-X, Lai Y-C. Predicting phase and sensing phase coherence in chaotic systems with machine learning. *Chaos* 2020;30(8):083114. <https://doi.org/10.1063/5.0006304>.
- [30] Carroll TL. Using reservoir computers to distinguish chaotic signals. *Phys Rev E* 2018;98(5):052209. <https://doi.org/10.1103/PhysRevE.98.052209>.
- [31] Krishnagopal S, Girvan M, Ott E, Hunt BR. Separation of chaotic signals by reservoir computing. *Chaos* 2020;30(2):023123. <https://doi.org/10.1063/1.5132766>.
- [32] Lu Z, Pathak J, Hunt B, Girvan M, Brockett R, Ott E. Reservoir observers: Model-free inference of unmeasured variables in chaotic systems. *Chaos* 2017;27(4):041102. <https://doi.org/10.1063/1.4979665>.
- [33] Nakai K, Saiki Y. Machine-learning inference of fluid variables from data using reservoir computing. *Phys Rev E* 2018;98(2):023111. <https://doi.org/10.1103/PhysRevE.98.023111>.
- [34] Chen X, Weng T, Yang H. Synchronization of spatiotemporal chaos and reservoir computing via scalar signals. *Chaos Solitons Fractals* 2023;169:113314. <https://doi.org/10.1016/j.chaos.2023.113314>.
- [35] Weng T, Chen X, Ren Z, Yang H, Zhang J, Small M. Synchronization of multiple mobile reservoir computing oscillators in complex networks. *Chaos Solitons Fractals* 2023;177:114217. <https://doi.org/10.1016/j.chaos.2023.114217>.
- [36] Zimmermann RS, Parlitz U. Observing spatio-temporal dynamics of excitable media using reservoir computing. *Chaos* 2018;28(4):043118. <https://doi.org/10.1063/1.5022276>.

- [37] Thiede LA, Parlitz U. Gradient based hyperparameter optimization in echo state networks. *Neural Netw* 2019;115:23–9. <http://dx.doi.org/10.1016/j.neunet.2019.02.001>.
- [38] Gonon L, Ortega J-P. Reservoir computing universality with stochastic inputs. *IEEE Trans Neural Netw Learn Syst* 2019;31(1):100–12. <http://dx.doi.org/10.1109/TNNLS.2019.2899649>.
- [39] Hoerl AE, Kennard RW. Ridge regression: Biased estimation for nonorthogonal problems. *Technometrics* 2012;12:55–67. <http://dx.doi.org/10.1080/00401706.1970.10488634>.
- [40] Huang C, Cui X, Di Z. Competition of spiral waves in heterogeneous CGLE systems. *Nonlinear Dynam* 2019;98:561–71. <http://dx.doi.org/10.1007/s11071-019-05212-1>.
- [41] Barkley D, Kness M, Tuckerman L. Spiral-wave dynamics in a simple model of excitable media: The transition from simple to compound rotation. *Phys Rev A* 1990;42:2489–92. <http://dx.doi.org/10.1103/PhysRevA.42.2489>.
- [42] Shepelev IA, Vadivasova TE. Variety of spatio-temporal regimes in a 2D lattice of coupled bistable FitzHugh-Nagumo oscillators. Formation mechanisms of spiral and double-well chimeras. *Commun Nonlinear Sci Numer Simul* 2019;79:104925. <http://dx.doi.org/10.1016/j.cnsns.2019.104925>.
- [43] McWilliam JA. Fibrillar contraction of the heart. *J Physiol* 1887;8(5):296. <http://dx.doi.org/10.1113/jphysiol.1887.sp000261>.
- [44] Xiao J, Hu G, Yang J, Gao J. Controlling turbulence in the complex Ginzburg-Landau equation. *Phys Rev Lett* 1997;81(25). <http://dx.doi.org/10.1103/PhysRevLett.81.5552>.